Biomechanical Analysis of a Novel Bioactive Dental Implant

Alexandre Varo Leal Salústio
alexandre.salustio@tecnico.ulisboa.pt

Instituto Superior Técnico, Lisboa, Portugal

October 2019

Dental implants are inserted into the jawbone to support a dental prosthesis in order to replace missing tooth. However, after the implantation, the sensory function of the mechanoreceptors originally located at the root is lost, which has been related to health complications and implant failure. Therefore, the development of a smart dental implant able to read the bite forces by means of an integrated sensor is a possible solution. The objective of this study was to investigate which regions at the implant-abutment interface (IAI) are more suited to welcome the sensor. A standard implant geometry was produced using computer-aided design software and then imported into finite element software, where different loading conditions based on mastication were used, and the resulting stress distribution along twelve points from two target regions was analyzed. The relation between stress at points from the top region and both the load angle and load magnitude was approximately linear, with the ones closest to the mesiodistal axis having distinctive response to the load angle, whereas the points at the bottom exhibited poor linearity and weak sensitivity to the load angle compared to the later. Thus, the top of the IAI appears to be more adequate for a sensor to detect changes in both the direction and magnitude of the bite forces. However, a more realistic geometry of bone and prosthesis is needed to reinforce the applicability of the study by improving the stress predictions.

Keywords: Dental Implant; Finite Element; Piezoelectric Sensor; Loading Conditions; Implant-abutment Interface; Internal Hex

I. INTRODUCTION

Dental implants are medical components implanted into the jawbone which support a dental prosthesis to overcome edentulism[1]. Once the tooth is extracted, the periodontal ligaments and periodontal mechanoreceptors (PMRs) are removed[2]. These receptors signal information on the forces applied to the teeth[3]. Thus, after the surgical implantation, teeth that have been replaced by dental implants lose their sensory function, and bite forces are no longer detected, which may be problematic if several adjacent teeth are replaced[4]. The reflex control of the masticatory system, which sets the bite force and jaw alignment, depends on PMRs[5]. PMRs have also been associated to the regulation and adjustment of body posture[6]. Hence, their absence compromises the proper running of these mechanisms, which might lead to implant overloading and bone loss due to stress shielding[7], or even changes in the running pattern[8]. Cognitive and mental diseases have also been linked to damaged or absent PMRs due to lack of trigeminal nerve and cortical area stimulation[9].

One possible solution to overcome the loss of PMRs is to develop a smart dental implant that includes force sensors which read changes in the bite forces, and then communicates with the nervous system though the same neural pathways involving PMRs. Pereira *et al*[10] proposed a prototype for the electronics of such device, using a piezoelectric sensor to detect well defined forces within the physiological range. However, the magnitude of the force at the sensor may be very different from the one applied to the tooth, given that the sensor should not be placed on the crown directly, but inside the implant, in which stress is non-uniformly distributed and depends on its geometry, materials and loading conditions.

The present study was conducted to analyze which regions of the implant-abutment interface (IAI) are more suited to welcome the sensor, such that the stress magnitude and distribution at those regions is related to the magnitude and direction of the bite force, and to describe that relation in both qualitative and quantitative terms.

II. METHODS

II.1 3D modelling

Computer-aided design (CAD) software was used to construct the model of the implant and surrounding bone, in the light of previous literature[11], and the crown restoration was added after specifications from an anatomical book[12]. Both implant and abutment were symmetric about both mesiodistal and buccolingual axes, whereas the crown was symmetric only about the buccolingual axis. **Figure 1** shows the 3D model used in this study, along with the most relevant dimensions. The geometry was then imported into a commercial finite element (FE) software.

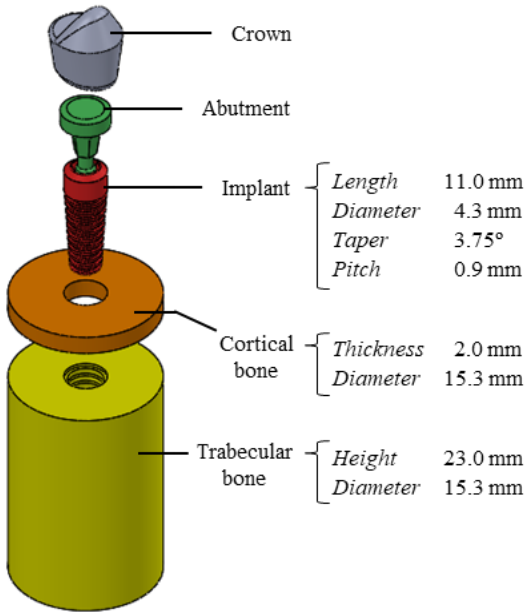

Figure 1. 3D CAD model of the implant system and surrounding bone.

II.2 Material properties

The properties of the cortical and trabecular bones, implant, abutment and crown were applied after previous literature[11,12]. All materials in the simulation were homogeneous, isotropic and linear elastic, thus described by the elastic modulus (E) and the Poisson ratio (ν) (**Table 1**).

Table 1. Material mechanical properties of the FE model.

Part (material)	E (GPa)	ν
Cortical bone	14.0	0.30
Trabecular bone	1.5	0.30
Implant (titanium grade IV)	114.0	0.37
Abutment (titanium alloy)	113.8	0.34
Crown (porcelain)	68.9	0.30

II.3 Boundary conditions and mesh

The outer bottom and lateral surfaces of bone were constrained in all directions[10,12,13]. The interface of the cortical and trabecular bones, bones and implant, and abutment and crown were applied as tie contact, which simulates perfect osseointegration, with the implant being fully integrated so that relative motion in the implant-bone interface is not possible[10,12,13]. The IAI was applied as frictional contact, with a friction coefficient of 0.5[10,14].

Edge and surface partitioning were employed all over the model to ensure symmetry after meshing. Based on the results of the convergence analysis, an element size of approximately 0.3 mm was used, giving a model with a total 174981 quadratic tetrahedral elements (**Figure 2**).

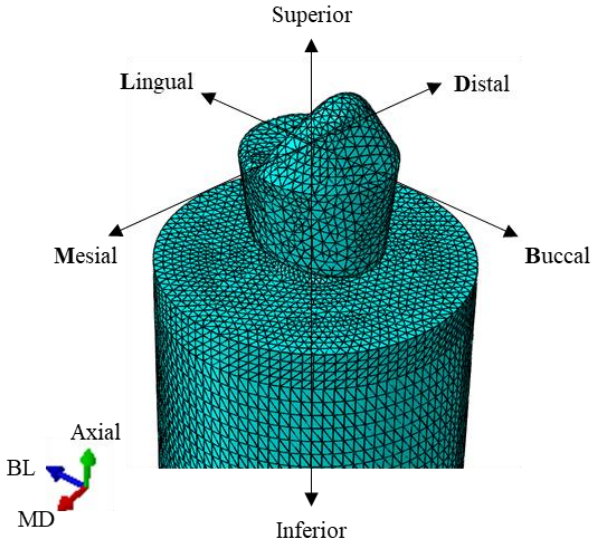

Figure 2. Top of the meshed FE model and global axes system.

II.4 Loading conditions

Two different loading conditions were used in this study: 1) static loads of 100 and 300 N were applied over the crown occlusal surface with angles to the axial axis ranging from 0º to 90º (**Figure 3**); 2) two dynamic loads (**Figure 4**), one with static magnitude (200 N) and varying angle, and other with both varying magnitude and angle, were applied over the same occlusal surface as before in order to simulate mastication[12]. An additional axial preload of 200 N mimicking the implant insertion[16] was considered for dynamic loading.

II.5 Validation of the model

The maximum Von Mises stress of cortical and trabecular bone under 0º, 15º, 30º and 60º loads of 100 N was

compared to that of a work with similar 3D model and FE features[11]. Furthermore, the Von Mises stress distribution at the top of the implant and abutment was also compared to that of the same work. The results were qualitatively close although the absolute value of the stress was slightly lower for this study's model. Therefore, the interpretation of further results should be exclusively qualitative rather than absolute.

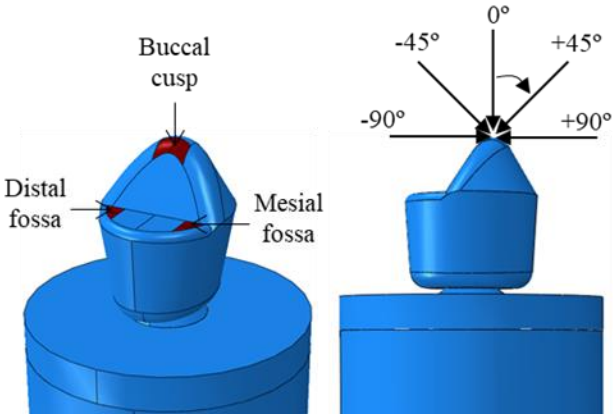

Figure 3. Occlusal surface (*left*) and load angle (*right*). The total load magnitude (100 and 300 N) was divided by three at each point of application.

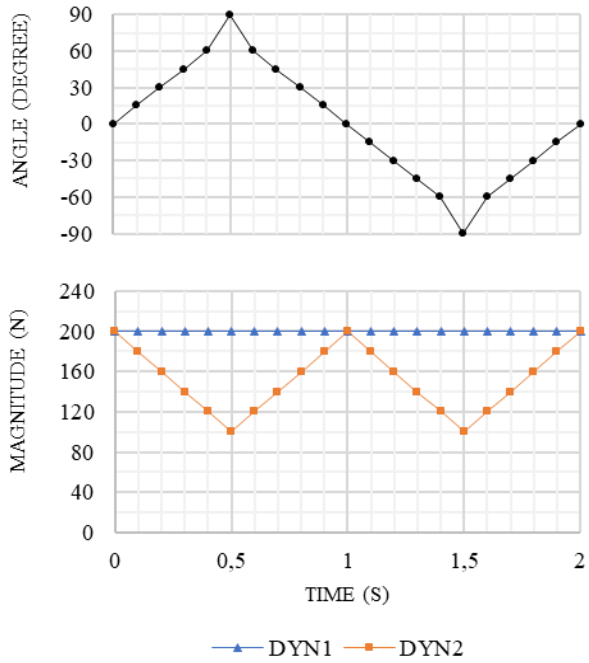

Figure 4. Time plot of the dynamic loads (DYN1 and DYN2) used in the second part of the analysis. (*top*) Angle plot, the same for both loads. (*bottom*) Magnitude plot.

II.6 Selection of target regions of the IAI

Two regions (top and bottom) of the IAI were selected as target regions after the remaining were ruled out due to theoretical incompatibilities with sensor placing space requirements and the fact that piezoelectric sensors usually read normal rather than shear forces. Six points of interest were chosen for each region. Bottom region points were labeled as "B1–6" and top region points were labeled as "T1–6", where the index is small for lingual points and great for buccal points (except for the pairs {2,3} and {4,5} which have the same buccolingual coordinate). These points are displayed on **Figure 5**.

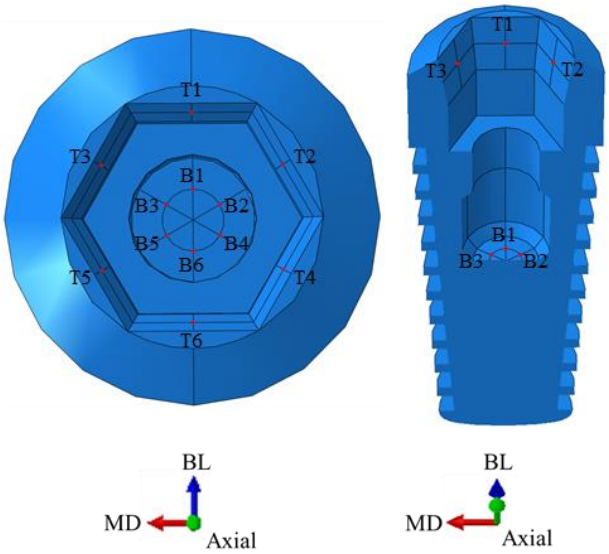

Figure 5. Target regions and points of interest. (*left*) Occlusal view of the implant. (*right*) Buccal view cut of the implant.

II.7 Stress outputs used in the analysis

Three stress-based scalar outputs were used in the analysis: Von Mises equivalent stress, average absolute compressive (AVGAC) stress and maximum absolute principal (MAXAP) stress. AVGAC stress is equal to the average of the modulus of the three normal stress components of the stress tensor and intends to inform on the compressive stress. However, because the face orientation may not match exactly the global coordinate system from which the stress tensor is calculated, the MAXAP stress was also analyzed, given it measures the maximum normal stress that can be measured at a point, regardless the orientation of the global axes.

II.8 Stress analysis

The variation of each stress output was studied under the first loading conditions among the twelve points of interest, in order to find patterns that exclusively relate the stress at a point to the bite force angle. In turn, the relation between the stress output and the bite force magnitude was assumed to be approximately linear given the linearity of

the material properties. The points with most distinctive stress-angle relation were considered the most suited to welcome the piezoelectric sensor.

Secondly, Von Mises stress was measured at the late selected points under the second loading conditions. Their stress performance was observed against the bite force in order to verify that changes in the force angle and magnitude were reflected on the stress at those points, and thus the choice was correctly done.

III. RESULTS AND DISCUSSION

III.1 Stress variation with the load angle

The plot results for Von Mises, AVGAC and MAXAP stress at the points of interest with the load angle were qualitatively similar, thus only the results for Von Mises are displayed.

Figure 6 shows the Von Mises stress variation with the load angle at the bottom points for a bite force of 100 and 300 N magnitude. The difference between the results for different magnitudes is practically just a scale factor and the same pattern can be observed for each point at both magnitudes, which indicates that the hypothesis of linearity between stress and the load magnitude is correct. Moreover, the results between points with the same buccolingual coordinate are essentially the same, which in turn indicates that the symmetry about the buccolingual axis was preserved after the meshing process. In addition, lingual points have slightly higher stress than buccal points for the 0º load, which is due to the asymmetry about the mesiodistal axis of both the crown and the occlusal surface. Then, as the load angle increases none of the bottom points increases or decreases monotonically. This result rules the bottom points out of the selection process, as the stress and the load angle are not exclusively related.

Figure 7 shows the Von Mises stress variation with the load angle at the top points for a bite force of 100 and 300 N magnitude. Once more, the results for points with the same buccolingual coordinate are very close, which demonstrates the aforementioned symmetry about the buccolingual axis. However, although the difference between the results for the two magnitudes still relies

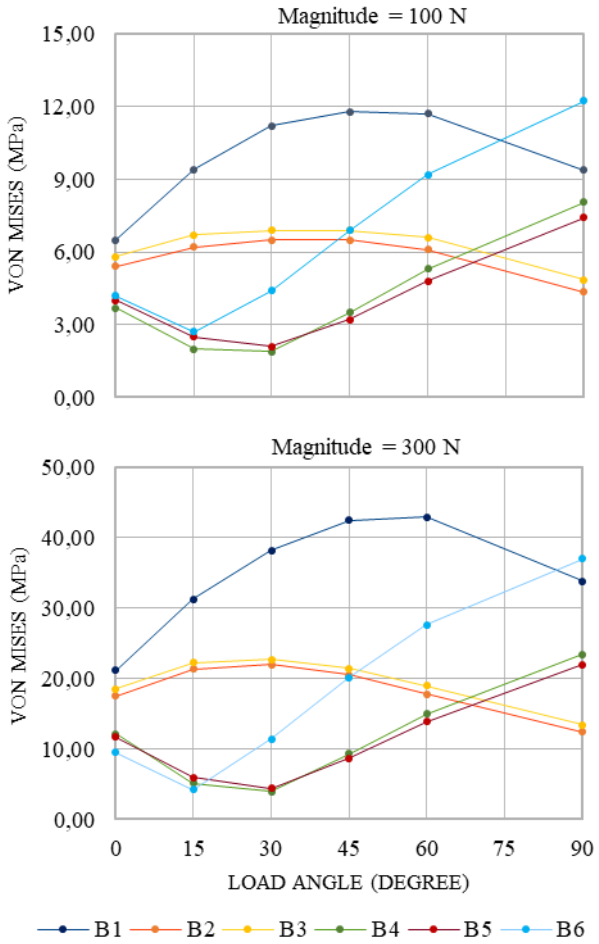

Figure 7. Variation of the Von Mises stress at the bottom points with the load angle. (*top*) 100 N load. (*bottom*) 300 N load.

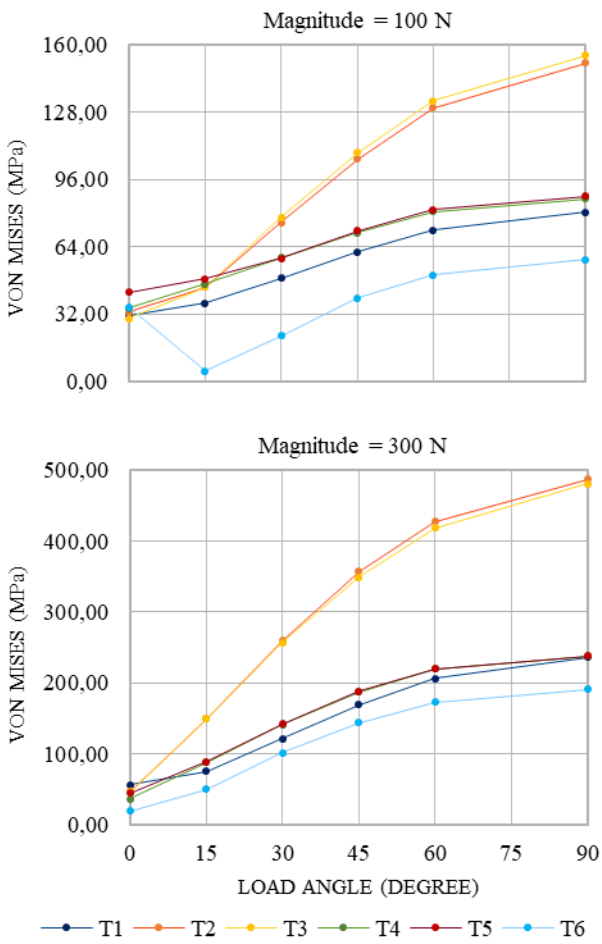

Figure 6. Variation of the Von Mises stress at the top points with the load angle. (*top*) 100 N load. (*bottom*) 300 N load.

majorly on a scale factor, the shape of the curves for the points T2/3 and especially T6 changed. This is not surprising as the top points are much closer to the occlusal surface, being exposed to greater stress, and the non-linear effects from the friction contact are thus more evident for this region. In contrast to the bottom region, the stress increases monotonically with the load angle overall, except for the point T6 under lower magnitudes. Moreover, points T2/3, which are located at the side where the force is pointing towards, have the most distinctive stress response to the load angle, mainly for greater loads, which can be observed by comparing the slope of the curves. This implies that these points are the ones with better sensitivity to the load angle, a property of interest to the placement of the sensor.

III.3 Linearity hypothesis

The relation between the stress and the load angle showed to be approximately linear for top points, with the slope being similar among points T1, T4/5 and T6 and significantly higher for T6, and the stress at 0º load angle was approximately the same among all points comparing to the rest of the angles. In order to test this hypothesis, linear equations on the form of a straight line equation were assigned to each point through linear regression modelling. The buccolingual symmetry of the model has been shown, hence the results for the pairs {B2,B3}, {B4,B5}, {T2,T3} and {T4,T5} were averaged and treated as on. Thus, 48 equations were defined for the curves corresponding to the eight points, two magnitudes and three stress outputs. The variables of the straight line equation were named after their mechanical meaning:

$$S_{P,M}(\theta) = SENS_{P,M}\ \theta\ +\ S_{0,P,M}$$

$$\begin{aligned} &S \in \{VM, MAXAP, AVGAC\}\ (MPa) \\ &M \in \{100, 300\}\ (N) \\ &P \in \{B1, B23, B45, B6, T1, T23, T45, T6\} \\ &0 \le \theta \le 90° \end{aligned} \qquad (1)$$

$S_{P,M}(\theta)$ is the stress outcome at a point P under a load with magnitude M and angle θ. $S_{0,P,M}$ is the stress outcome at that point under a 0º load of magnitude M, and should be approximately equal among the points of each region. $SENS_{P,M}$ is the slope of the curve and indicates the point sensitivity to the load angle, being zero if changing the load angle does not affect the stress outcome at that point. The degree to which each curve is accurately modelled by its regression equation is associated to the respective coefficient of determination (R^2). R^2 ranges from 0 to 1 and it can be thought as the percentage of points of the original curve that fall within the results of the line formed by the regression equation.

Table 2 shows the results for the R^2 of the 48 equations. R^2 averages less than 0.60 for bottom points and about 0.86 for top points. Points T2/3 and T4/5 alone average a R^2 of about 0.91. This means that stress at top points is significantly more linear than for bottom points, which has already been observed before, and points T2/3 and T4/5 have the highest linearity compared to the rest, which makes them good candidates for welcoming the sensor for now. Given their low R^2, bottom points cannot be meaningfully described by Equation 1, and therefore results for $SENS_{P,M}$ and $S_{0,P,M}$ are shown for the top points only.

Table 2. Results of R^2. Each column features a color scale where red and green were set to match the minimum and maximum values, respectively.

Output	*Von Mises*		*MAXAP*		*AVGAC*	
Magnitude	100 N	300 N	100 N	300 N	100 N	300 N
B1	0,22	0,32	0,70	0,69	0,24	0,28
B2/3	0,21	0,43	0,01	0,58	0,41	0,27
B4/5	0,63	0,55	0,88	0,89	0,74	0,65
B6	0,90	0,91	0,97	0,95	0,95	0,93
T1	0,97	0,96	0,96	0,95	0,94	0,91
T2/3	0,96	0,94	0,97	0,95	0,98	0,96
T4/5	0,95	0,92	0,96	0,92	0,54	0,92
T6	0,56	0,93	0,50	0,92	0,17	0,92

Table 3 contains the parameter $SENS_{P,M}$ of the top points. On the one hand, T2/3 have the greater $SENS_{P,M}$ among the top points, confirming that the T2/3 are more sensitive to the load angle than the rest. On the other hand, $SENS_{P,M}$ of T2/3 is on average three times greater than that for T4/5. This means that, under positive-angled loads, stress at both T2/3 and T4/5 increases linearly with the angle, but three times as fast for T2/3. One may infer that, due to the overall symmetry about the mesiodistal axis, the results for T2/3 under positive-angled loads would be the same or close to that for T4/5 under negative-angled loads and vice-versa.

Table 3. Results of $\boldsymbol{SENS_{P,M}}$ for the top points. Each column features a color scale where red was set to match $\boldsymbol{SENS_{P,M} \leq 0.10}$ and green was set to be the maximum value of the column.

Output	*Von Mises*		*MAXAP*		*AVGAC*	
Magnitude	100 N	300 N	100 N	300 N	100 N	300 N
T1	0,59	2,18	0,71	2,78	0,32	1,25
T2/3	1,47	5	1,66	5,68	0,67	2,42
T4/5	0,58	2,28	0,51	2,23	0,09	0,73
T6	0,45	2,03	0,44	2,05	0,1	0,68

Table 4 shows the results for $S_{0,P,M}$. In general, lingual points have higher stress at 0º loads, which is clearer for loads with greater magnitude. This result comes from the small asymmetry of the occlusal surface (**Figure 3**), whose centroid is slightly lingual.

Table 4. Results of $\boldsymbol{S_{0,P,M}}$ for the top points. Each column features a color scale where red and green were set to match the minimum and maximum values, respectively.

Output	*Von Mises*		*MAXAP*		*AVGAC*	
Magnitude	100 N	300 N	100 N	300 N	100 N	300 N
T1	31,61	56,69	34,18	49,39	21,68	32,87
T2/3	32,19	85,5	36,73	81,04	20,13	24,03
T4/5	40,87	61,31	43,64	59,42	18,61	21,1
T6	16,87	31,46	19,46	35,3	10,85	15,43

The results from Tables 2, 3 and 4, and the assumption of buccolingual symmetry indicate that points T2/3 and T4/5 may be used together to detect changes in the load angle. T2/3 is more sensitive to positive angles, whereas T4/5 is more sensitive to negative angles. When the load angle is equal to 0º, the stress outcome is close between points.

III.4 Combination of the stress outputs into a single signal

Equation 1 may be transformed into a more general equation describing the Von Mises stress at a given point under a load with a given angle and magnitude, by passing *M* as a second argument of the equation instead. Moreover, as discussed before, because the materials are linear elastic, the magnitude of the load can be approximated to act merely as a global scale factor. The stress at a 0º load angle may be also considered the same for top points. Therefore, a new equation is derived, where points T2/3 correspond to the index "+" and T4/5 correspond to the index "–":

$$\begin{aligned} &VM_P(\theta, M) = f_P(\theta) g(M) \\ &= (SENS1_P(\theta)\,|\theta| + VM_0)\, SENS2\, M \\ &P \in \{+, -\} \\ &-90º \leq \theta \leq 90°, 100 \leq M \leq 300\ N \end{aligned} \tag{2}$$

where,

$$\begin{aligned} SENS1_+(\theta) &\propto \begin{cases} 1, & \theta > 0° \\ 1/3, & \theta < 0° \end{cases} \\ SENS1\_(\theta) &\propto \begin{cases} 1/3, & \theta > 0° \\ 1, & \theta < 0° \end{cases} \\ SENS2 &\in IR^+ \end{aligned} \tag{3}$$

The stress at the points T2/3 will be detected by the piezoelectric sensor into an electric signal which is directly proportional to it, say S^+. In turn, S^- is the electric signal from the points T4/5. These two signals may be combined into one single output signal that carries the information on the load angle and magnitude alone. By making use of the linearity observed for these two points and their differential sensitivity to the load angle sign, two algebraic expressions come readily to mind: subtraction and quotient.

S_{DIFF} is the differential output equal to S^+ minus S^-. According to Equation 2, S_{DIFF} is defined as

$$\begin{aligned} &S_{DIFF}(\theta, M) \propto VM_+(\theta, M) - VM\_(\theta, M) \\ &= \left(SENS1_+(\theta) - (SENS1\_(\theta)\right)|\theta| SENS2\, M \end{aligned} \tag{4}$$

From Equation 3 and 4, S_{DIFF} is deduced to have the same sign as the load angle. For a 0º load, S_{DIFF} is approximately 0. Furthermore, under loads of static magnitude, the absolute value of S_{DIFF} increases linearly with the load angle. Also, as it would be expected, under static angles, increasing the magnitude of the load also increases S_{DIFF} linearly. The major advantage of considering S_{DIFF} is that it is easily configured, and that if one of the properties of the load is static, the other can be linearly detected. However, as its value can increase due to changes in both direction and amplitude of the load, it may not be ideal under fully dynamic loads.

S_{QUO} is the quotient between S^+ and S^-. From Equation 2, it is defined as

$$S_{QUO}(\theta, M) \propto VM_+(\theta, M)/VM_-(\theta, M) = \frac{SENS1_+(\theta)\,|\theta| + VM_0}{SENS1_-(\theta)\,|\theta| + VM_0} \quad (5)$$

It is straightforward that S_{QUO} does not depend on the load magnitude as the parcels $SENS2\,M$ cancel each other. Moreover, for a 0º load angle, S_{QUO} is 1. For positive load angles, as $SENS1_+(\theta)$ is greater than $SENS1\_(\theta)$, S_{QUO} is greater than 1. The same reasoning can be done for negative load angles, where S_{QUO} is proportionally smaller than 1. Furthermore, it can be inferred that for higher angles, S_{QUO} becomes $SENS1_+(\theta)/SENS1\_(\theta)$ which is a constant that can be equal to two values, one greater than 1 and other that is its inverse, for positive and negative load angles, respectively. S_{QUO} is thus not able to detect changes in the load magnitude but may serve the detection of the sign of the load angle and even its value, although it is not as clear as in S_{DIFF}, where the relation was linear. Therefore, if the load is expected to be highly dynamic in both direction and magnitude, S_{QUO} might be employed.

III.5 Assessment of the choice of points T2/3 and T4/5 using dynamic loads

Von Mises stress at the top points the resulting S_{DIFF} and S_{QUO} from T2/3 and T4/5 were analyzed under dynamic loading. The results for the semi-static load DYN_1 are shown on **Figures 8** and **9**, and the results for the full-dynamic load DYN_2 are shown on **Figures 10** and **11**.

III.5.1 Dynamic load 1

The results shown on **Figure 8** confirm the hypothesis that points T2/3 and T4/5 have the most linear response to the load angle as they have the stress curve that most resembles the load angle curve (**Figure 4**). Furthermore, the stress at T2/3 is higher than at T4/5 for positive angles ($0 \leq t \leq 1$ s) and the difference between them increases and decreases in agreement with the load angle. The opposite happens between T4/5 and T2/3 for negative angles, confirming the buccolingual symmetry of the stress at the top points when the sign of the load angle is reversed. Moreover, points T1 and T6 are displayed, and the lower linearity of the point T6 at positive load angles and of the point T1 at negative load angles predicted on **Table 2** is visible on **Figure 8**.

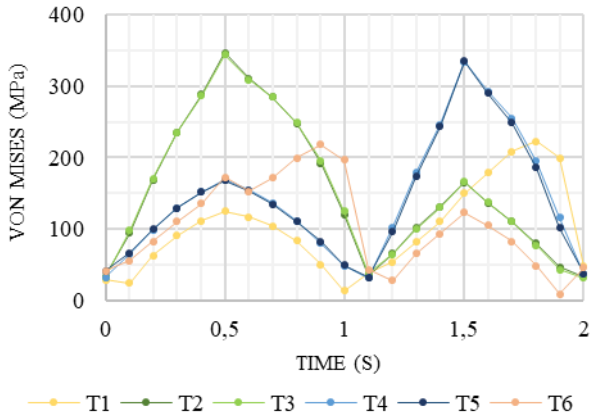

Figure 8. Von Mises stress at the top points under load DYN_1.

Figure 9 shows the output signals S_{DIFF} and S_{QUO} for DYN_1. One the one hand, as expected, the sign of S_{DIFF} agrees with that of the load angle and increasing the load angle also increases S_{DIFF}. On the other hand, S_{QUO} is bigger than 1 for positive angles and smaller than 1 for negative angles. However, the shape of the S_{QUO} curve does not resemble that of the load angle, having a step shape instead, that converges to a constant value greater or smaller than one when the load angle is positive or negative, respectively.

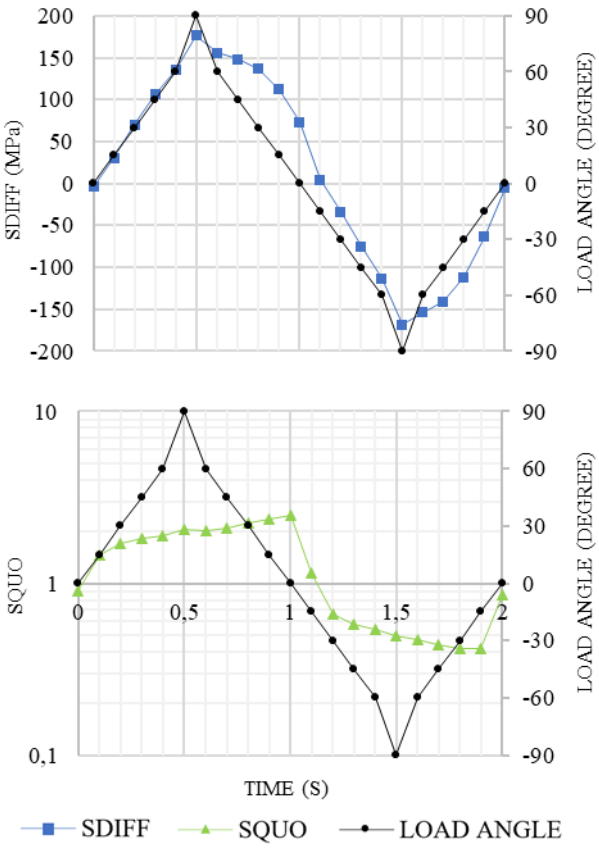

Figure 9. S_{DIFF} and S_{QUO} signals and load angle for load DYN_1.

III.5.2 Dynamic load 2

The results for Von Mises at the top points are shown on **Figure 10**. On the one hand, T2/3 and T4/5 have once more the most linear response to the load angle. Secondly, the Von Mises magnitude at these points decreased compared to DYN_1. This is due to the magnitude profile of the load, which decreases from 200 N to 100 N in the interval 0–0.5 s and at 1–1.5 s (**Figure 4**). As the magnitude profile is symmetric in each one of the two steps, the stress response to the load angle remains uncorrupted in a way that the stress is higher for higher load angles. This can be can also be observed on the signal S_{DIFF}.

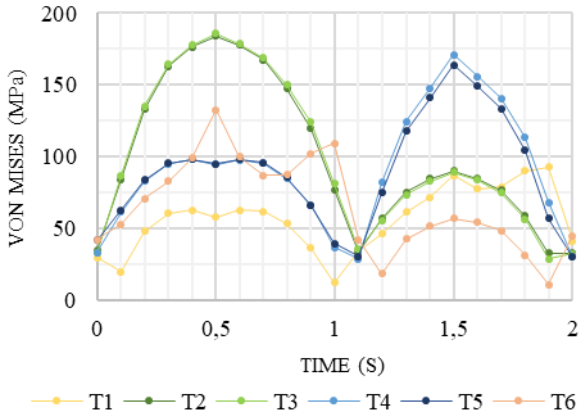

Figure 10. Von Mises stress at the top points under load DYN_2.

S_{DIFF} (**Figure 11**) is again positive for positive angles and negative for negative angles, and it increases and decreases in agreement with the load angle, although the absolute value of S_{DIFF} is reduced comparing to DYN_1, again in conformity with the load magnitude decrease. Nevertheless, it is important to discuss what would happen if the magnitude of the load was not symmetric within each step and, for instance, it was continuously decreasing from 200 N to, say, 0 N in each step. As the magnitude appears to function as a scale factor to the stress, the stress curve would not be symmetric anymore and the right side of the parables that can be seen for T2/3 and T4/5 at 0–1 s would not be similar to the left side. Because of the continuously decreasing magnitude, the right side of the parable would decrease, but faster. This rapid decrease could erratically lead to the interpretation that the load angle was also decreasing faster than for the left side. This is the major concern when dynamic magnitude is considered, with S_{DIFF} being changed by both the load angle and the magnitude.

As for S_{DIFF}, the interpretation of S_{QUO} (**Figure 11**) is also similar to that done for DYN_1, with values higher (lower) than 1 occurring for positive (negative) angles.

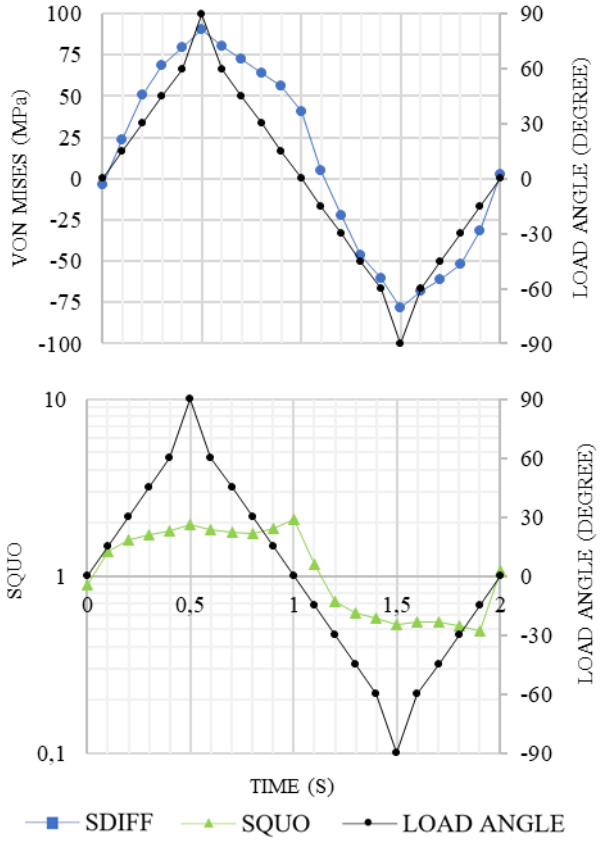

Figure 11. S_{DIFF} and S_{QUO} signals and load angle for load DYN_2.

The big difference between S_{QUO} and S_{DIFF} is that the values for S_{QUO} are closer to each other between DYN_1 and DYN_2 compared to S_{DIFF}. As only the magnitude changes from DYN_1 to DYN_2, it is safe to assume that S_{QUO} is considerably less sensitive to the magnitude than S_{DIFF}, which in turn suggests that the assumption made for Equation 3, that treats the stress function as a simple product composition between an angle-sensitive factor and a global magnitude-sensitive factor, is correct.

Thus, several output signals may be chosen accordingly to the objective of the sensor and the expected loading conditions at the tooth. If static magnitudes or static angles are anticipated, S_{DIFF} is sufficient to read changes in the load direction and magnitude, respectively. In the case of full dynamic loads, S_{QUO} may be used to detect the sign of the load angle, although more complex algebraic combination of the signals from T2/3 and T4/5 may be required to isolate the desired properties.

IV. CONCLUSIONS

Within the limitations of this study, two major conclusions can be drawn: 1) the stress within the top region of the IAI is linearly related to both the load angle and magnitude, especially for points located at the mesiodistal faces of the hexagonal connection; 2) among the later, the stress at buccal (lingual) points is highly sensitive to loads towards the buccal (lingual) side of the crown, and about three times less sensitive to loads towards the buccal (lingual) side. This symmetry allowed for the proposition of single outputs combining signals from points at each side of the mesiodistal axis, from which the load magnitude and angle might be retrieved. Thus, the development of a smart dental implant that includes a force sensor in order to reestablish the sensory function of the natural tooth should address the top region of the IAI, where the stress outcome closely relates to the properties of the bite load, and simple single output signals can be derived from the outputs of the sensors at each point that inform on the variation of these properties.

However, the simulation of more realistic geometries and the inclusion of the piezoelectric sensors in the model would help to improve the applicability of the later conclusions and even allow a more precise, quantitative analysis.

V. Acknowledgments

This paper and the research behind it would not have been possible without the assistance of my supervisors, Professors André Castro and Paulo Fernandes, and the overall support from Instituto Superior Técnico.

VI. References

1. Warreth, Abdulhadi & Ibieyou, Najia & O'Leary, Ronan & Cremonese, Matteo & Abdulrahim, Mohammed. (2017). Dental implants: An overview. Dental Update. 44. 596-620.
2. Malet, J., Mora, F. & Bouchard, P. (2018). Implant dentistry at a glance. Hoboken, NJ: Wiley.
3. Piancino, M. G., Isola, G., Cannavale, R., Cutroneo, G., Vermiglio, G., Bracco, P., & Anastasi, G. P. (2017). From periodontal mechanoreceptors to chewing motor control: A systematic review. Archives of Oral Biology, 78, 109–121.
4. Türker, K. S., Sowman, P. F., Tuncer, M., Tucker, K. J., & Brinkworth, R. S. A. (2007). The role of periodontal mechanoreceptors in mastication. Archives of Oral Biology, 52(4), 361–364.
5. Trulsson, M. (2006). Sensory-motor function of human periodontal mechanoreceptors. Journal of Oral Rehabilitation, 33(4), 262–273.
6. Cuccia, A., & Caradonna, C. (2009). The relationship between the stomatognathic system and body posture. Clinics, 64(1).
7. Zhao, Y., Wang, W., Xin, H., Zang, S., Zhang, Z., & Wu, Y. (2013). The remodeling of alveolar bone supporting the mandibular first molar with different levels of periodontal attachment. Medical & Biological Engineering & Computing, 51(9), 991–997.
8. Maurer, C., Stief, F., Jonas, A., Kovac, A., Groneberg, D. A., Meurer, A., & Ohlendorf, D. (2015). Influence of the Lower Jaw Position on the Running Pattern. PLOS ONE, 10(8)
9. Mastication and cognitive function. (2011). Dental Abstracts, 56(4), 211–214.
10. Pereira, B. A. (2018). Dental Pressure Detection and Nerve Stimulation Demonstration Prototype (Master's thesis).
11. Chun, Heoung-Jae & Shin, Ha-Shik & Han, Chong-Hyun & Lee, Soo-Hong. (2005). Influence of implant abutment type on stress distribution in bone under various loading conditions using finite element analysis. The International journal of oral & maxillofacial implants. 21. 195-202.
12. Okeson, J. (2012). Management of Temporomandibular Disorders and Occlusion.
13. Alper, B., Gultekin, P., & Yalci, S. (2012). Application of Finite Element Analysis in Implant Dentistry. Finite Element Analysis - New Trends and Developments.
14. Geng, J.-P., Tan, K. B. C., & Liu, G.-R. (2001). Application of finite element analysis in implant dentistry: A review of the literature. The Journal of Prosthetic Dentistry, 85(6), 585–598.
15. Jafarian, M., & Emadi, N. (2019). Finite element analysis of stress distribution around a dental implant with different amounts of bone loss: An in vitro study. Dental and medical problems, 56(1), 27-32.
16. Massoumi, F., Taheri, M., Mohammadi, A., & Amelirad, O. (2018). Evaluation of the Effect of Buccolingual and Apicocoronal Positions of Dental Implants on Stress and Strain in Alveolar Bone by Finite Element Analysis. Journal of dentistry (Tehran, Iran), 15(1), 10–19.